Organic Process Research & Development

Article

pubs.acs.org/OPRD

Investigation of Batch Cooling Crystallization in a Liquid−Liquid Separating System by PAT

Huaiyu Yang[†] and Åke C. Rasmuson*[,†,‡]

[†]Department of Chemical Engineering and Technology, Royal Institute of Technology (KTH), SE-100 44 Stockholm, Sweden

[‡]Department of Chemical and Environmental Science, Solid State Pharmaceutical Cluster, Materials and Surface Science Institute, University of Limerick, Limerick, Ireland

ABSTRACT: Crystallization of butyl paraben from water−ethanol mixtures has been investigated. The liquid−liquid phase separation and the solid−liquid solubility have been determined from 1 to 50 °C. Cooling crystallizations have been performed at different starting compositions, and the processes have been recorded by in-situ infrared spectroscopy, focused beam reflectance measurement, and particle video microscopy. In pure water the butyl paraben solubility is below 1 mg/g, while in pure ethanol the solubility is more than 3 orders of magnitude higher. While the solution saturated with butyl paraben is homogeneous at 1 °C, at the higher temperatures butyl paraben induces a liquid−liquid phase separation of the ethanol−water mixture, and the ternary phase diagram contains up to five different regions. The size of the liquid−liquid phase separation region increases with increasing temperature. At 50 °C, even the binary butyl paraben water system separates into two different liquid phases. In the cooling crystallizations, the resulting product crystals and the behavior of the process are quite different, depending on the starting composition. The largest crystals and the least agglomeration were obtained in that experiment where liquid−liquid phase separation was not occurring. In all of the other experiments the crystals were smaller and more agglomerated, and the particle size distribution was wider or more irregular. The work illustrates how Process Analytical Technology (PAT) can be used to increase the understanding of complex crystallizations.

INTRODUCTION

Crystallization from solution is a method central to the production of a wide range of chemical products, e.g. organic fine chemicals and pharmaceuticals. To understand and control the crystallization process it is essential to establish the phase diagram, in particular in more complex cases like solvent mixtures, racemic mixtures, and cocrystals. While, binary solvent mixtures are commonly used in industrial crystallizations, the corresponding ternary phase diagrams are not well explored and neither is the crystallization behavior in systems exhibiting liquid−liquid phase separation. In one example though, spherical crystallization is carried out in solvent mixtures and often near the liquid−liquid phase separation boundary.[1,2] The morphology of polymer blends is largely determined by the interplay between liquid−liquid phase separation (LLPS) and crystallization.[3,4] When liquid−liquid phase separation occurs within the metastable zone during crystallization, it can have a great impact on the crystallization process.[5] The liquid−liquid phase separation makes crystallization difficult in systems that include protein.[6] The liquid−liquid phase separation hinders both primary and secondary nucleation in crystallization of droplets.[7] During the past decade the application of process analytical technology (PAT) has increased substantially and has been used in researching liquid−liquid phase separation and crystallization processes by methods such as focused beam reflectance measurement (FBRM),[8] in-situ infrared spectroscopy (IR),[9] particle video microscopy (PVM),[10] dielectric constant measurement,[11,12] bulk video imaging,[8,13] in-situ Raman spectroscopy[14] and statistical control chart-based methods.[15,16]

In the present study, we have investigated the system of butyl paraben (BP)−ethanol−water. It turns out that in a certain temperature range, butyl paraben enforces a liquid−liquid phase separation in the ethanol−water mixture. Although the solubility of butyl paraben in different solvents has been studied,[17−19] to the best of our knowledge, the conditions in water−ethanol mixtures have not been investigated previously. In addition, liquid−liquid phase separation has not been extensively investigated[18,19] in relation to industrial crystallization.[20,21] The aim of this work is to investigate the phase and crystallization behavior of the ternary system butyl paraben + water + ethanol in the temperature range 1−50 °C. We report the direct observation of the liquid−liquid phase separation and the determination of solid−liquid solubility of butyl paraben. Solutions with different proportions of butyl paraben, water, and ethanol have been crystallized under the monitoring of in-situ FBRM, PVM, and FTIR.

Parabens are alkyl esters of *p*-hydroxybenzoic acid. They have a relatively low toxicity, and the compounds or their salts are the most common preservatives in use today and found in thousands of cosmetics, toiletries, food, and pharmaceutical products.[22−26] Antimicrobial activity and the octanol−water partitioning coefficient increase with increasing molecular weight and, hence, length of the alkyl side chain.[27−29] Combinations of parabens appear to have synergistic effects on bacteria;[28,30] hence, as a preservative, methyl paraben is often used in combination with one or more of ethyl-, propyl-, and butyl-paraben.[31] Perlovich[32] has investigated the thermodynamics of parabens, and Giordano[33] and Feng[34,35] have determined the

Received: December 5, 2011
Published: May 21, 2012

dx.doi.org/10.1021/op200355b | *Org. Process Res. Dev.* 2012, 16, 1212−1224

crystal structures and studied the relationship to physical properties.

MATERIALS AND METHODS

Materials. Butyl paraben (with melting point 67−70 °C cited on the package) of purity >99.0% by mass was purchased from Aldrich and was used without further purification. Ethanol (99.7% by mass) was purchased from Solveco chemicals from VWR, and distilled water was used.

Procedures. *Solubility of Paraben.* The solubility of butyl paraben in the temperature range 1−50 °C was determined by the gravimetric method in pure water and pure ethanol, and in 10%, 30%, 50%, 70%, and 90% by weight ethanol (on solute-free basis) in ethanol−water mixtures. The temperature was controlled by thermostat baths with uncertainty of ±0.01 °C. The temperature measurements have been calibrated against a mercury precision thermometer (Precision, Germany) with uncertainty of ±0.01 °C).

Solutions were prepared in 200 mL bottles. To about 50 mL of solvent in each bottle at 10 °C was added solid butyl paraben in excess of the solubility. Saturation was reached by dissolution, assuring there was solid phase in the solution at equilibrium. The solutions were kept under agitation 400 rpm for more than 12 h to ensure that equilibrium had been established. The agitation was then turned off, and the solid material was allowed to settle for half an hour. A 10 mL syringe in its unbroken plastic bag was put into the water bath for several minutes in order to reach the same temperature as the solution. Then the syringe with needle

Table 1. Proportions (weight percent) of butyl paraben, water, and ethanol in 5 experiments

experiment no.	proportion of butyl paraben (%)	proportion of water (%)	proportion of ethanol (%)
1	64.6	0	35.4
2	53.3	17.4	29.3
3	44.3	19.3	36.4
4	29.9	45.6	24.5
5	11.7	58.2	30.1

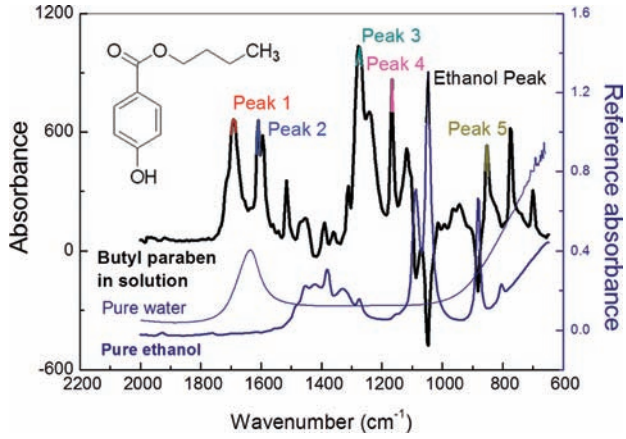

Figure 2. Infrared spectra for the butyl paraben solution, pure ethanol, and pure water, respectively. The spectra for butyl paraben is the resulting spectra after subtraction of the pure ethanol spectra.

Table 2. Wavenumbers of five IR peaks of BP and one peak of the ethanol and the related function groups[36]

peak no.	wavenumber (cm^{-1})	group
1	1690	−C═O
2	1599	$-COO^-$
3	1280	−CH, −C−O−
4	1166	−C−C−, −C−O−
5	852	$-CCH_{aromat}$, −COC−
ethanol peak	1020	ethanol, −C−O−

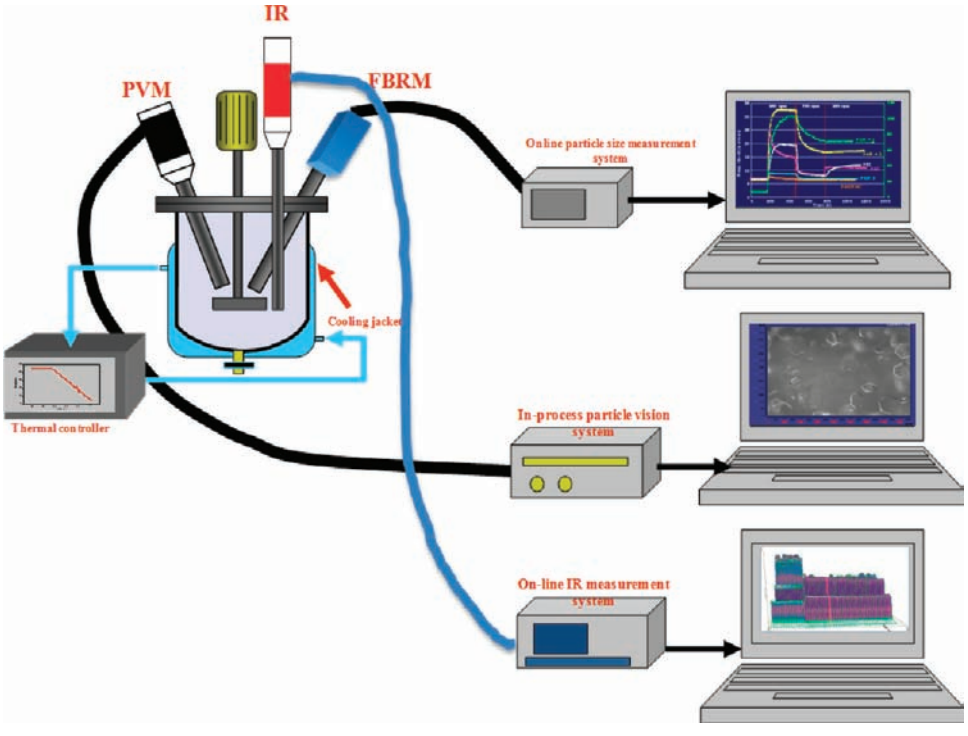

Figure 1. Equipment for the cooling crystallization experiments in the ternary phase diagram (temperature control, FBRM, IR, and PVM).

dx.doi.org/10.1021/op200355b | *Org. Process Res. Dev.* 2012, 16, 1212−1224

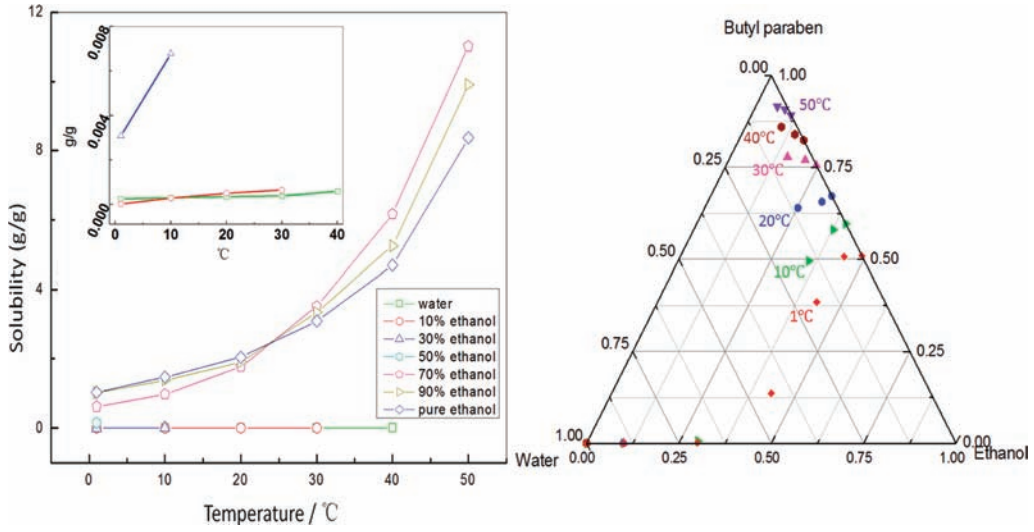

Figure 3. Solubility of butyl paraben in ethanol−water solutions at different temperatures.

was used to sample (2−4 mL) the solution in the bottles. A filter (PTFE 0.2 μm) was attached to the syringe through which the solution was distributed into two small preweighed plastic bottles (1−2 mL each). Each bottle was quickly covered to prevent evaporation and weighed with its contents. The cover was then removed, and the samples were dried in ventilated laboratory hoods at room temperature (about 25 °C). The solid residue mass was recorded repeatedly throughout the drying process to complete dryness. Sometimes more than a month was required since the solid phase tended to form a cake at the liquid surface, thus slowing down the evaporation. (Every day the cake was mechanically broken, to sustain the evaporation.) The weight of the final dry sample was used for calculation of the solubility, of course with appropriate correction for the weight of the cover. The balance (Mettler AE 240) used during the experimental work had a resolution of ±0.00001 g. The different steps were repeated for every 10 °C interval up to 50 °C.

Liquid−Liquid Phase Separation. The ternary phase diagram of butyl paraben, water, and ethanol was investigated at 1, 10 , 20, 30, 40, and 50 °C. A 300 mL glass bottle with plastic cover was put in the thermostat bath, the temperature of which was controlled with an uncertainty of ±0.01 °C. The balance (Tamro HF-300G, A&D Company) used during the experiment work had a resolution of ±0.001 g.

The different regions were explored by addition of butyl paraben, water, or ethanol step by step. First, at 20 °C a starting point in the ternary phase diagram was selected, and a 100 mL mixture of butyl paraben, water, and ethanol with desired proportions was prepared in a 500 mL glass bottle. The solution was stirred by a magnetic stirrer at 200 rpm. Then, one of the components, butyl paraben, water, or ethanol, was added into this solution step by step, allowing 30 min of equilibration at each step, until a different phase appeared (for example the clear solution changed to cloudy or undissolved solid butyl paraben began to form in the solution). Then, the other two components were added in smaller steps to revert back to the previous phase region. The phase boundary is defined as being between two steps back and forth where the phase separation is established to occur. The process of adding different materials was repeated to clarify the location of the phase boundary more exactly. Repeating this procedure from different starting points in the ternary diagram established the properties of the full phase diagram, which had been done for six different temperatures: 1, 10, 20, 30, 40, 50 °C, with an estimated uncertainty less than 1%.

Cooling Crystallization. Five different cooling crystallization experiments are reported with different proportions of butyl paraben, water, and ethanol (Table 1). From experiment 1 to 5, the proportion of water increases and the proportion of butyl paraben decreases. In the five experiments, the solutions were heated to 45 °C and equilibrated for 30 min, after which the solutions were cooled down to 5 °C at the rate of −0.1 °C min^{-1}. In experiment 4, a solution of composition equal to experiment 3 was heated to 45 °C, and then 200 g water was added at the rate of 1 g min^{-1}, resulting in the composition of experiment 4 given in the table.

Cooling crystallizations were performed in a Mettler Toledo Labmax, Figure 1. The solution was mixed in a 1 L jacketed, unbaffled, cylindrical glass crystallizer and was agitated at 200 rpm. The temperature and agitation in the crystallizer were controlled and observed by iControl Labmax version 4.0. The crystallization was monitored using in-situ IR, FBRM, and PVM. The IR probe (React IRTM diamond ATR composite) with a measurement range from 2000 to 0 cm^{-1} was operated with measurement duration 2 s and was controlled by icIR version 4.0. The FBRM probe (D600L version), with a measurement range of 0.25−2000 μm, was operated with a measurement duration 2 s and was controlled by icFbrm version 4.0. Five population ranges, 0−5 μm, 5−40 μm, 40−120 μm, 120−500 μm, and 0−1000 μm, were used. The PVM probe (model 700) was operated with an image update rate of 6 images per minute, obtaining in situ photos of 600 μm × 800 μm.

Five peaks of butyl paraben and one peak of ethanol (Figure 2 and Table 2) were used to record changes of the composition. The IR spectrum of ethanol has been subtracted from that of the butyl paraben (Software icIR 4.0); however, the water spectrum does contribute especially to peak 5 at 852 cm^{-1}. The ethanol peak has not been corrected for the overlap with the butyl paraben peak at the same wavelength. Additional experiments have been performed at essentially the same conditions in a similar stand-alone, 1 L jacketed, glass crystallizer to determine the product weight distribution by sieving (Fritsch GmbH BRD - 6580) using the sieves, 50 μm, 100 μm, and every 100 μm step up to 1100 μm.

dx.doi.org/10.1021/op200355b | *Org. Process Res. Dev.* 2012, 16, 1212−1224

RESULTS AND DISCUSSION

Solubility and the Phase Diagram. The solubility of butyl paraben in ethanol−water mixtures from 1 to 50 °C are shown in Figure 3 and are given in Table 3. In pure water and even with 10 wt % ethanol (on solute-free basis) the solubility is below 0.01 g/g. The mole fraction solubility of butyl paraben in pure water at 20 °C is 3.2×10^{-5}, which is a higher than the value of found by Grant[37] (about 2.1×10^{-5} at 20 °C) and the value found by Allexander[38] (about 2.3×10^{-5} at 25 °C). The differences are attributed to the solubility being very low. However, in previous solubility research,[39] the solubility of butyl paraben in ethanol is consistent with literature values. At 30% ethanol the solubility is about 5 times higher than in pure water, and the temperature dependence is much stronger. However, already at 10 °C liquid−liquid phase separation occurs. In pure ethanol and in mixtures with a moderate concentration of water the paraben solubility is very high. At 70% ethanol and above there is no liquid−liquid phase separation in the temperature range investigated.

Diagrams a−f of Figure 4 show the ternary phase diagrams of butyl paraben, water and ethanol at 1, 10, 20, 30, 40, and 50 °C, respectively. Points denote experimental observations, and lines are the best attempt to identify phase boundaries. From 10 to 40 °C, there are five regions in the diagram. Region 1 is an undersaturated (with respect to paraben) homogeneous solution. In region 2, two liquid phases are in equilibrium; however, they are undersaturated with respect to butyl paraben. In region 3, a water-rich homogeneous liquid is saturated with butyl paraben. In region 4, solid paraben and two liquid phases are in equilibrium. In region 5, solid butyl paraben is in equilibrium with an ethanol-rich solution. The solution appears a bit yellow, resulting from the high concentration of butyl paraben.

Obviously the phase diagram shifts in a systematic way from 1 to 50 °C. At 1 °C, all regions but 1 and 3 are absent, and the diagrams only present a simple solid−liquid solubility curve. Already at 10 °C the diagram is much more complex, exposing all five regions, and the solid−liquid solubility line cuts through the liquid−liquid phase separation region (regions 2 and 4). At increasing temperature the liquid−liquid phase separation region expands gradually into the ethanol-lean part of the diagram, and the solid−liquid solubility curve of butyl paraben moves along with that. Region 1 (i.e. the region containing a homogeneus solution that is unsaturated with respect to butyl paraben) expands with increasing temperature. From 30 °C and upwards, region 4 decreases until it reached 50 °C where regions 3 and 4 have essentially disappeared. Along with these changes region 5, bound by the solubility curve of butyl paraben in an ethanol-rich solution and the liquid−liquid phase separation boundary, also gradually decreases in size with increasing temperature. One reason is that the concentration of butyl paraben in the ethanol-rich solution steadily increases with increasing temperature.

The regions 2, 4, and 5 that disappear are present at 10 °C but absent at 1 °C. When the temperature is cooled from 10 to 1 °C, the first region to disappear is region 2, and then region 4 after that. Simultaneously, regions 3 and 5 merge into one region. At 50 °C, there are only four regions—region 3 disappears above 40 °C. Region 4 is still present at 50 °C, however, only as a very thin region close to the water−butyl paraben axis. A water solution, with no ethanol, saturated by butyl paraben is homogeneous from 1 to 40 °C, but at 50 °C the system turns into a system of two liquid phases (an aqueous phase with a low concentration of butyl paraben and a second liquid phase with a high butyl

Table 3. Solubility (g solute/g solvent) of butyl paraben in weight percent 0−100% ethanol aqueous solution from 0.9 to 49.9 °C and standard deviation in brackets (− conditions with LLPS)[a]

	average solubility of butyl paraben (standard deviation)						
temperature (°C)	in water (g/g)	in 10% ethanol(g/g)	in 30% ethanol (g/g)	in 50% ethanol (g/g)	in 70% ethanol (g/g)	in 90% ethanol (g/g)	in ethanol[39] (g/g)
0.9	2.399×10^{-4} (7.78×10^{-6})	2.086×10^{-5} (4.53×10^{-6})	3.080×10^{-3} (7.57×10^{-5})	0.1580 (9.90×10^{-4})	0.6254 (5.85×10^{-3})	1.0315 (1.41×10^{-4})	1.0384 (2.27×10^{-3})
9.9	2.908×10^{-4} (2.42×10^{-5})	2.750×10^{-4} (2.33×10^{-5})	6.782×10^{-3} (1.16×10^{-4})	–	0.9809 (5.59×10^{-3})	1.3826 (3.39×10^{-4})	1.4780 (7.76×10^{-4})
19.9	3.478×10^{-4} (2.10×10^{-5})	5.009×10^{-4} (4.20×10^{-6})	–	–	1.7751 (3.46×10^{-2})	1.9095 (1.77×10^{-3})	2.0517 (3.06×10^{-2})
29.9	3.808×10^{-4} (1.05×10^{-5})	6.516×10^{-4} (5.30×10^{-6})	–	–	3.5127 (8.56×10^{-3})	3.3481 (1.57×10^{-2})	3.0896 (6.77×10^{-2})
39.9	5.884×10^{-4} (1.42×10^{-5})	–	–	–	6.1623 (2.21×10^{-2})	5.2472 (1.09×10^{-1})	4.6883 (2.51×10^{-2})
49.9	–	–	–	–	11.0118 (3.42×10^{-2})	9.9040 (2.67×10^{-2})	8.3645 (2.50×10^{-2})

[a]The measurement standard uncertainty, $u(w) = 0.00001$g, $u(T)$ is 0.01 K.

dx.doi.org/10.1021/op200355b | Org. Process Res. Dev. 2012, 16, 1212−1224

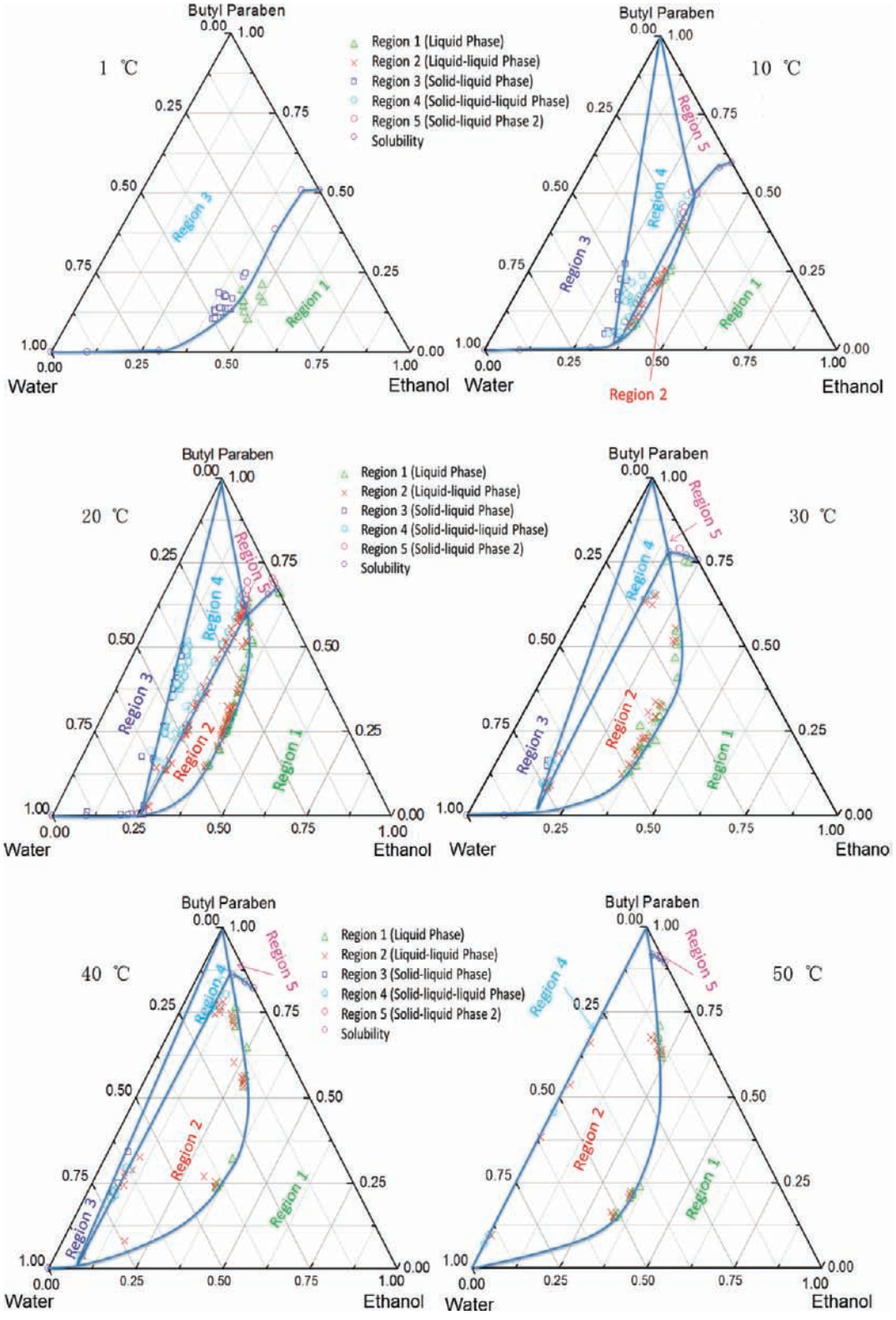

Figure 4. Ternary phase diagram of butyl paraben, water, and ethanol. From upper left to lower right: at 1 °C, 10 °C, 20 °C, 30 °C, 40 °C, and 50 °C.

paraben concentration). The liquid−liquid phase separation in the binary butyl paraben−water mixture above 40 °C has been previously reported.[37] In the case of no agitation, the butyl paraben-rich phase is floating on top of the water-rich phase. As opposed to many other systems where the liquid−liquid miscibility increases with increasing temperature,[40,41] in this case the liquid−liquid phase separation increases with increasing temperature. The results also reveal that at 1 °C, there is no liquid−liquid phase separation regardless of ethanol concentration, and the solubility of butyl paraben steadily increases with increasing ethanol concentration. At increasing temperature liquid−liquid phase separation gradually occurs at lower ethanol concentration. Accordingly, in a sense the miscibility between the water-rich phase and the ethanol-rich phase tends to decrease

dx.doi.org/10.1021/op200355b | *Org. Process Res. Dev.* 2012, 16, 1212−1224

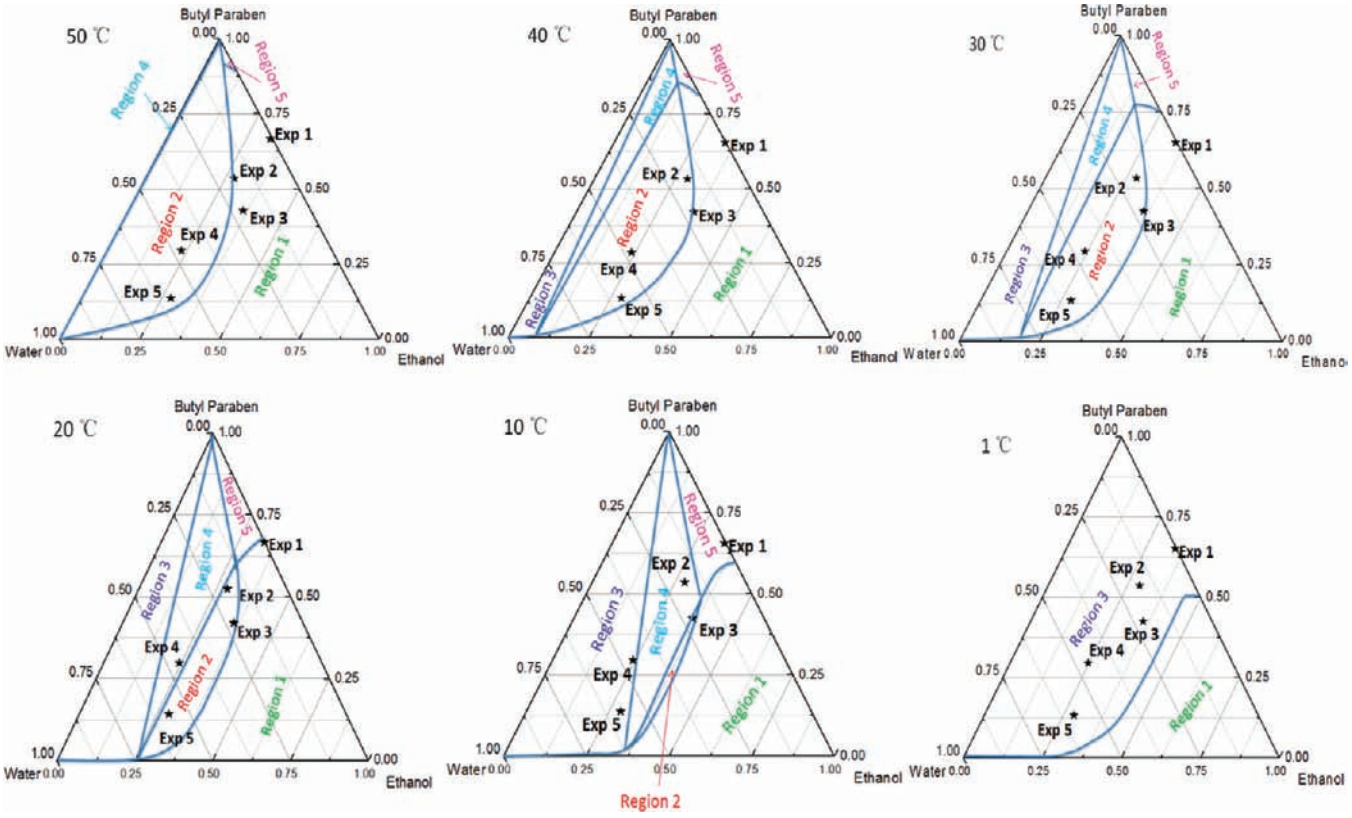

Figure 5. Composition points of five experiments in ternary phase diagram from 50 to 1 °C.

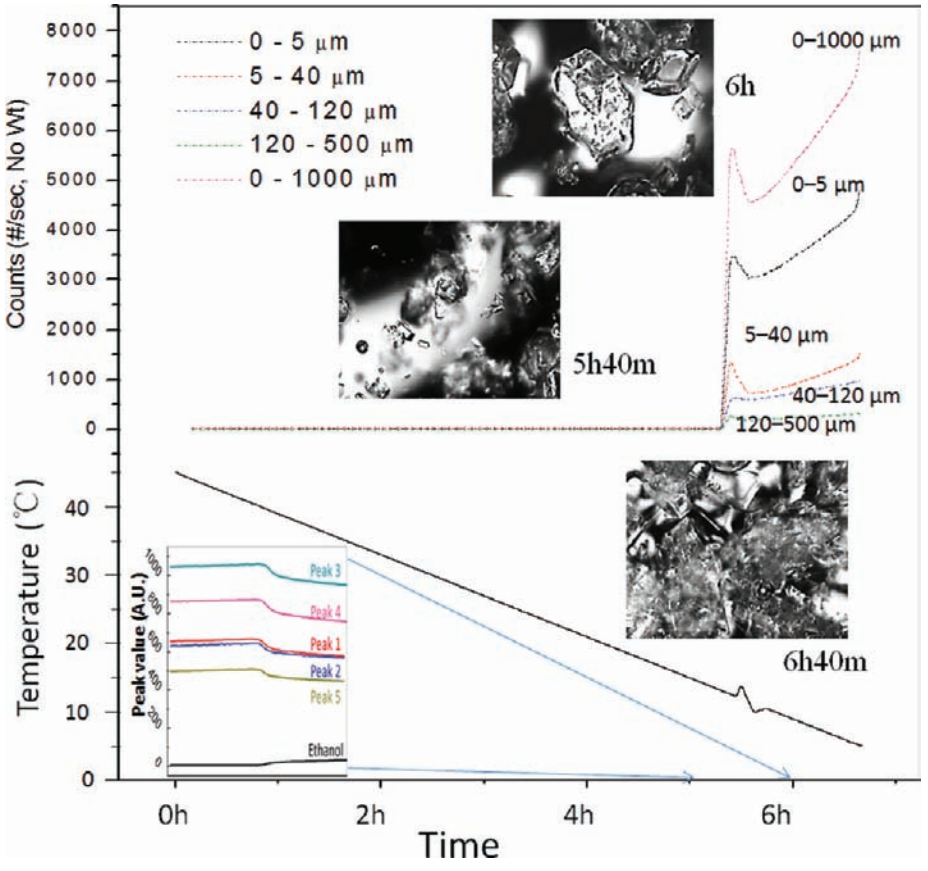

Figure 6. Temperature profile, FBRM curves, IR curves, and PVM photos of experiment 1.

dx.doi.org/10.1021/op200355b | *Org. Process Res. Dev.* 2012, 16, 1212–1224

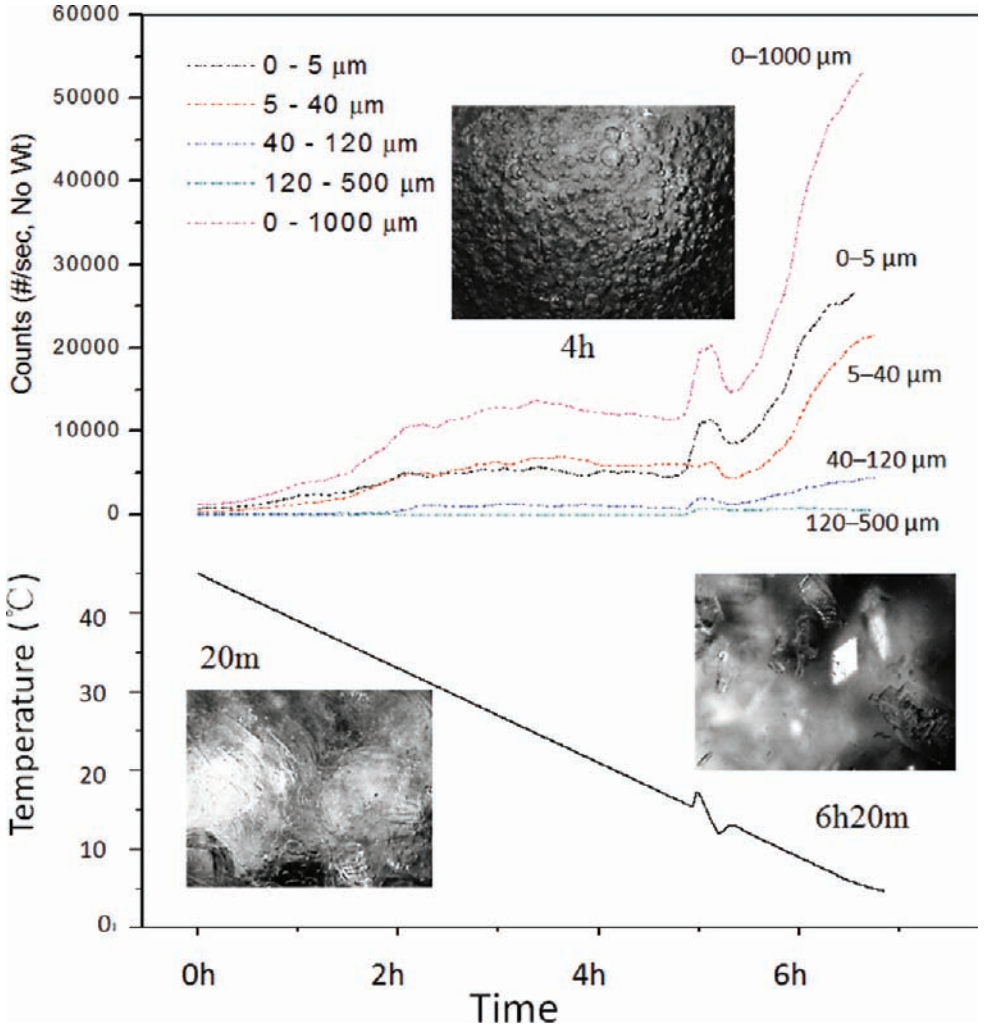

Figure 7. Temperature profile, FBRM curves, and PVM photos of experiment 2.

with increasing temperature. From 10 to 50 °C regardless of how much BP is added, there is no liquid–liquid phase separation when the ethanol concentration is above 70% weight (on solute-free basis). Similarly, regardless of BP concentration, there is no liquid–liquid phase separation at 10 °C when the ethanol concentration is less than about 37%, at 20 °C when the ethanol concentration is less than about 25%, at 30 °C when the ethanol concentration is less than about 20%, and at 40 °C when the ethanol is less than about 8%.

Cooling Crystallization. Figure 5 presents the starting point of each of the five cooling crystallization experiments in the ternary phase diagram and how they relate to the different regions at different temperatures from 50 to 1 °C. Figure 5 clearly shows how the cooling process changes the conditions for the mixture from the starting temperature of 45 °C to the final temperature of 5 °C. Experiment 1 started in the homogeneous region and never experienced liquid–liquid phase separation during the course of the process. Experiments 2 and 3 started as homogeneous solutions and experienced liquid–liquid phase separation before crystal nucleation occurred. Experiments 4 and 5 started as liquid–liquid-separated mixtures. During the cooling, crystal nucleation occurred, and both experiments ended as suspensions having a homogeneous liquid phase.

In the crystallization experiments, crystal nucleation can be distinguished from liquid–liquid separation primarily by the fact that crystallization is associated with a latent heat of phase transformation which leads to a small but clear peak in the temperature vs time profile. Furthermore, in the case of crystal nucleation the FBRM response increases rapidly, whereas in the case of liquid–liquid phase separation there is a slower increase. When nucleation occurs in a liquid–liquid phase-separated mixture, the number of crystals increases, while the number of droplets tends to decrease. The reason for the latter is that the liquid–liquid separation is actually due to the presence of the butyl paraben, and a reduced butyl paraben concentration tends to reduce the immiscibility. For experiments 2, 3, and 4, the number of crystals generated exceeds the reduction of the number of droplets, while for experiment 5, the opposite holds. In addition, crystal nucleation is always associated with a decrease in IR response, which is not necessarily true for liquid–liquid phase separation, and of course PVM helps to distinguish nucleation from liquid–liquid phase separation.

Experiment 1. The solution of experiment 1 started in region 1 of the ternary phase diagram, as an undersaturated paraben–ethanol solution. The solution nucleated when the cooling solution bypassed the solubility curve and "crossed over" to region 5, where the crystals finally grew. The process was an ordinary cooling crystallization in a homogeneous solvent, and the product size distribution was as expected from this type of process. The nucleation took place after about 5 h 20 min (PVM

dx.doi.org/10.1021/op200355b | *Org. Process Res. Dev.* 2012, 16, 1212–1224

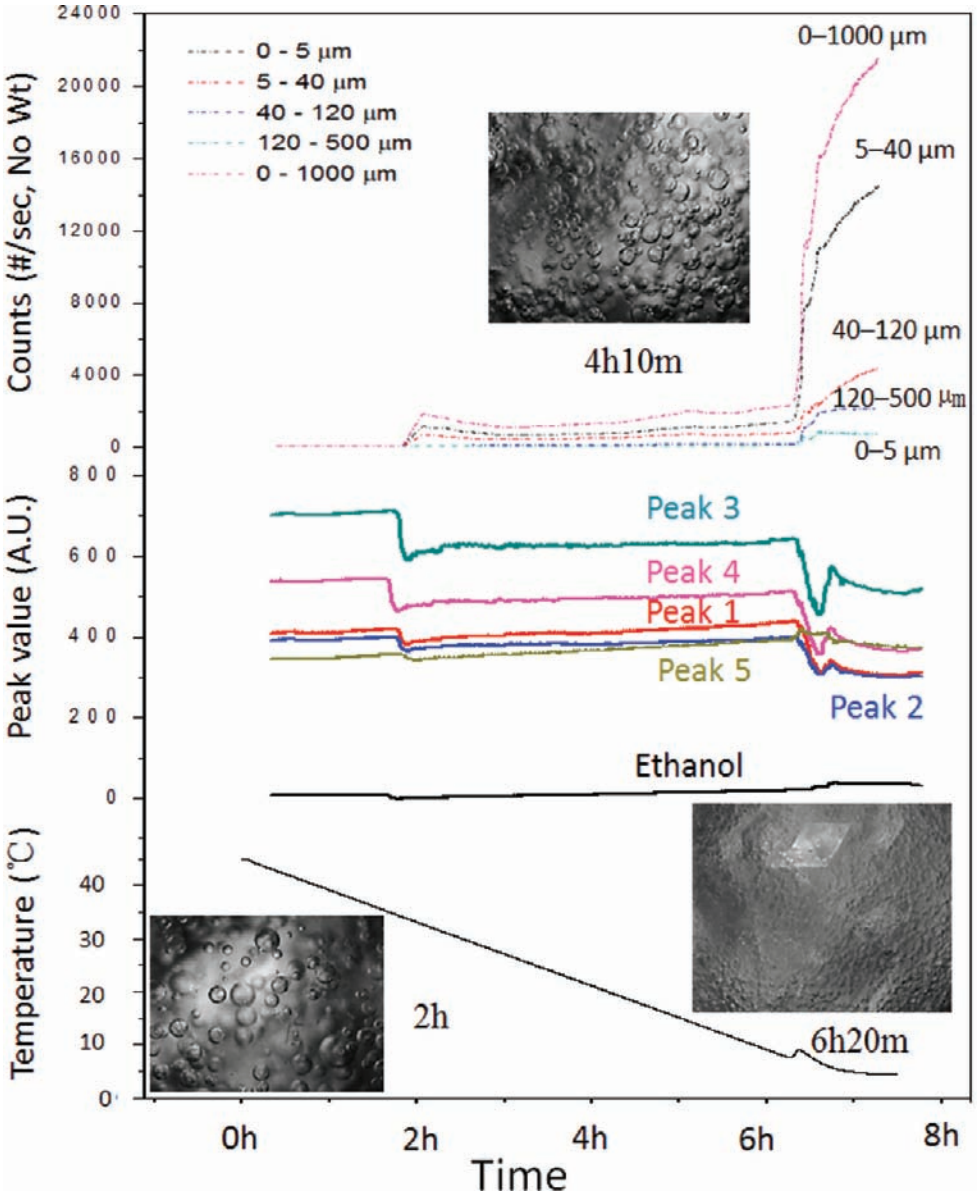

Figure 8. Temperature profile, FBRM curves, IR curves, and PVM photos of experiment 3.

photos in Figure 6), when the temperature reached about 15 °C. The nucleation was also accompanied by a temperature increase because of the heat liberated as a result of the enthalpy of crystallization. The temperature increase led to dissolution of some of the crystals, in particular the smaller ones shown as a sudden drop of the FBRM curves. During the cooling process ahead of nucleation, all the FBRM curves were close to zero, and the IR curves of butyl paraben increased slightly because of the decreasing temperature. When the temperature reached about 15 °C, the butyl paraben IR peaks revealed rapid reduction in the concentration of butyl paraben. However, the IR curve of ethanol increased, showing relatively increasing concentration of ethanol in the solution. After that the crystals grew in the supersaturated solution, and it appeared as if there was a contribution of secondary nucleation towards the end. At low temperature, some butyl paraben crystals adhered and grew on the glass surface of the PVM probe. During the whole process, the liquid remained nonturbid, meaning there was no liquid–liquid phase separation.

Experiment 2. The solution of experiment 2 started close to the liquid–liquid phase separation boundary between region 1 and region 2, in a mixture of water and ethanol having a paraben concentration somewhat less than that in experiment 1. At cooling, the solution passed into the LLPS region 2, and the formation of droplets could be observed by the PVM. At continued cooling, crystal nucleation occurred, the crystals grew in the LLPS region 4, and the process ended in region 3. The size distribution (Figure 11) is wide with a tendency of bimodality but is still reasonably well formed. The FBRM results (Figure 7) showed that the liquid–liquid phase separation occurred quite early. The PVM revealed the droplets formed in region 2, and visually the solution became quite turbid. Then with decreasing temperature the white turbidity became more intense, similar to that of milk. At about 18 °C, nucleation took place as was observed in the FBRM signals and by the increase of the temperature. After crystal nucleation the solution remained milk-white. More crystals were formed as the temperature decreased, and the process ended with a high concentration of crystals in region 3, which had no liquid–liquid phase separation. The PVM photos at the end reveal a homogeneous liquid phase with faceted crystals.

dx.doi.org/10.1021/op200355b | *Org. Process Res. Dev.* 2012, 16, 1212–1224

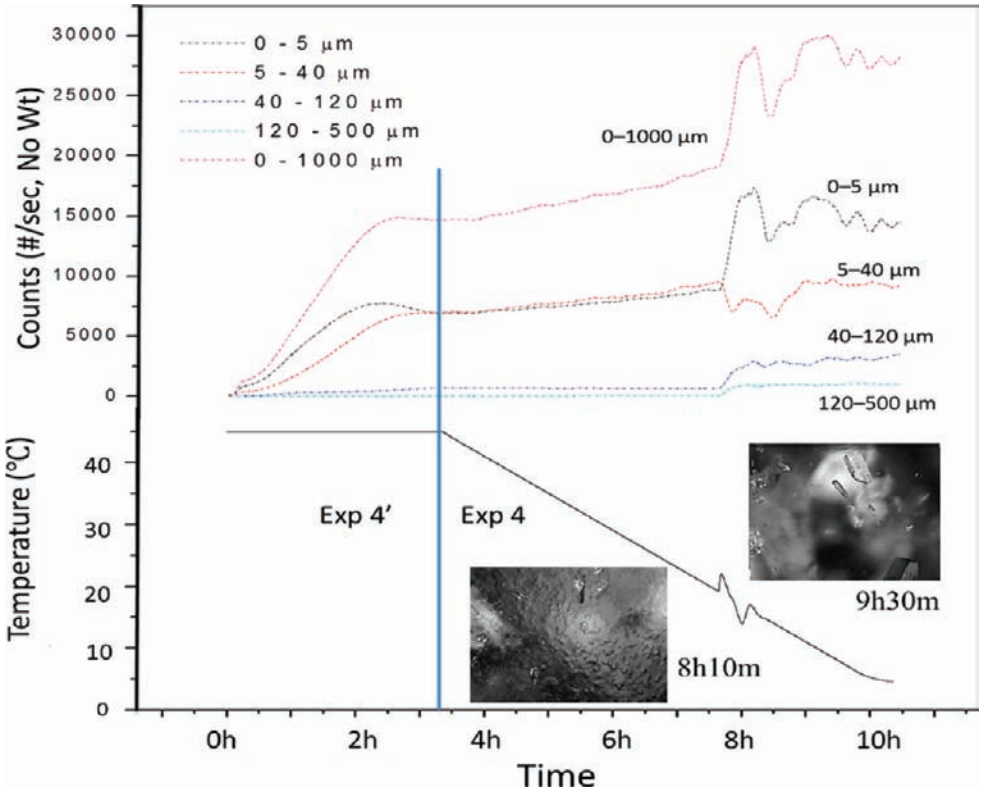

Figure 9. Temperature profile, FBRM curves, and PVM photos of experiments 4′ and 4.

Experiment 3. The solution of experiment 3 started more clearly inside region 1 and with a somewhat lower butyl paraben concentration than in experiment 2. Liquid–liquid phase separation occurred when the solution entered into the LLPS region 2 at about 35 °C, as was observed by both the PVM response as the solution became milk-white and by the FBRM data shown in Figure 8. In fact, this liquid–liquid phase separation can also be recorded in the FTIR data (Figure 8) in that the peaks of butyl paraben suddenly decreased. The liquid–liquid phase separation led to a dispersed phase enriched in butyl paraben and a continuous phase accordingly depleted in butyl paraben. The continuous phase appeared to be somewhat higher in ethanol concentration, since the ethanol peak remained unchanged in spite of the decrease of the overlapping butyl paraben peak. With decreasing temperature of the solution, the IR curves of butyl paraben and ethanol increased slightly. When the solution was further cooled into region 4, butyl paraben nucleated at about 10 °C as shown by the rapid increase in the FBRM curves and the exothermic temperature peak. The IR curves of peaks 1, 2, 3, and 4 clearly decreased while that of peak 5 actually increased somewhat, likely to be an effect of the changing concentration of water. Crystals formed, but the solution remained milk-white, which also showed in the PVM photos at various times, suggesting the formation of crystals in the LLPS solution. The crystals grew into the final product crystal size distribution in the liquid–liquid phase separation region, and towards the end, the solution contained a lot of small crystals but remained nontransparent because of the liquid–liquid phase separation. Obviously, the poor crystal size distribution in Figure 11 is related to crystal formation that took place and ended in a liquid–liquid phase-separated mixture.

Experiment 4. Experiment 4 was initially operated as an antisolvent process at 45 °C. The experiment started with a solution identical to that of experiment 3, to which was added 200 g of water that moved the composition into the liquid–liquid phase-separated region 2, as shown in Figure 4. At the water feeding point, the solution became milk-white, but this milky solution disappeared quickly again when mixed with the bulk solution. When more water was added, the rate of the disappearance of the milky solution became slower and slower, the region of milk-white solution became larger and larger, and the color became gradually more intense. Finally, the entire solution turned light-white then milk-white because of liquid–liquid phase separation throughout the entire volume. This is also revealed in Figure 9 by the increasing FBRM curves which show that the number of droplets continued to increase during the whole process of water addition. The addition of water not only generated liquid–liquid phase separation but also led to an overall reduction of the paraben concentration in the continuous liquid phase because of dilution and liquid–liquid phase separation.

After 200 min the addition of water terminated, and then the solution was cooled down as in the other experiments. When the temperature reached about 20 °C, the solution entered into region 4, and the number of particles rapidly increased since crystal nucleation was occurring. However, because of the corresponding temperature increase of the solution, this was followed by dissolution of some of the crystals, most clearly seen in the small size range. Interestingly, the number of particles in the range 5–40 μm show an immediate decrease at the crystal nucleation. This was interpreted as a change in droplet size distribution. After a short period, the number in the 5–40 μm range increased again as a result of crystal growth. The PVM photos at 8 h 10 min and 9 h 30 min show the crystal growth in region 4 with LLPS solution and in region 3 where the solution was homogeneous and the process was terminated, respectively.

dx.doi.org/10.1021/op200355b | *Org. Process Res. Dev.* 2012, 16, 1212–1224

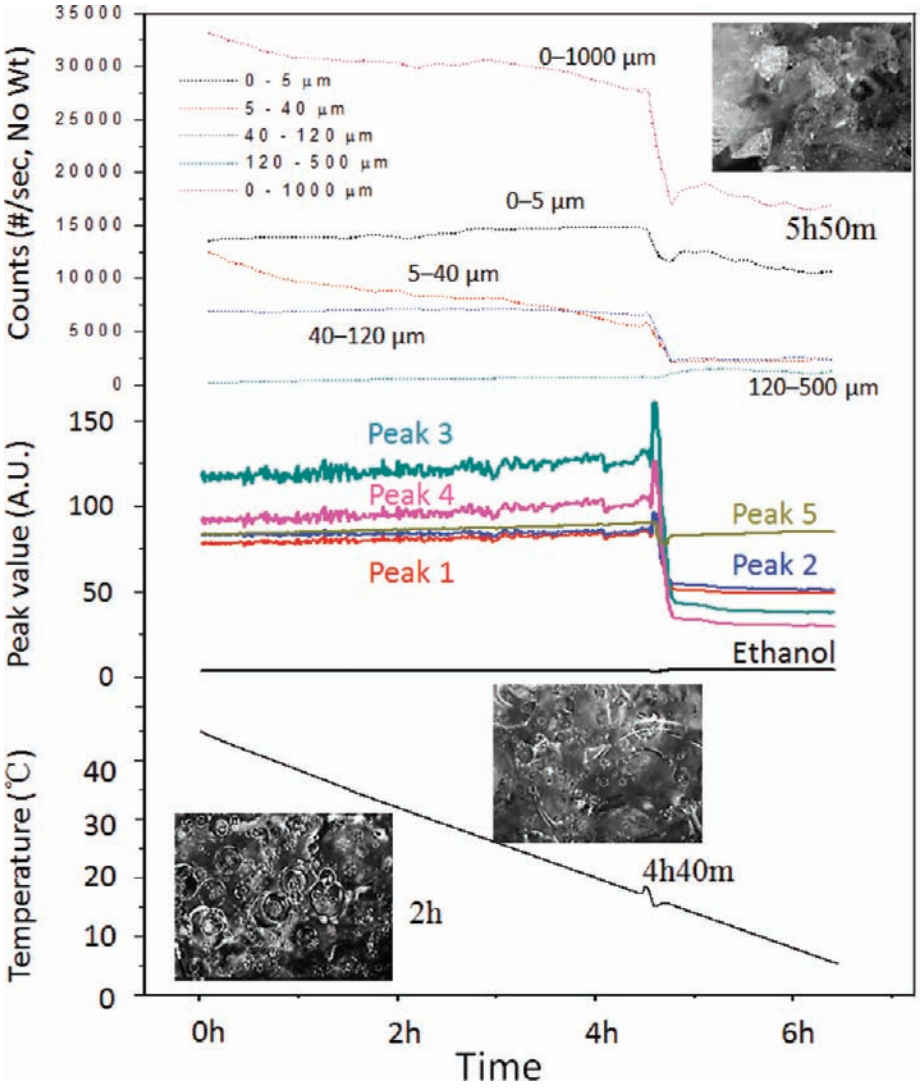

Figure 10. Temperature profile, FBRM curves, IR curves, and PVM photos of experiment 5.

The FBRM particle size distribution in Figure 11a is not very smooth. The crystals are comparatively small which is likely due to a stronger nucleation because of a lower solubility at the ending point. The material is not strongly agglomerated.

Experiment 5. The experiment 5 solution started in the LLPS region 2, having a butyl paraben concentration much less than in other experiments and having the highest water concentration of all. At cooling, the solution nucleated when passing into region 4, and by further cooling ended up in region 3. The FBRM curves (Figure 10) show that there was a liquid−liquid phase separation from the start. Crystal nucleation occurred at about 15 °C, surprisingly revealed by the number of recordings in the 0−5, 5−40, 40−120 intervals all suddenly decreasing quickly while the curve representing particles above 120 μm increased somewhat. The explanation for this is assumed to be the fact that butyl paraben is the component forcing a LLPS into a mixture of ethanol and water. When butyl paraben crystallizes out, the concentration of butyl paraben in the solution decreases, leading to an increase in the miscibility of the liquid phases and a redissolution of the droplets. Decreasing IR curves and FBRM curves both reveal the moment of nucleation in experiment 5. Peak 5 decreased less than the other peaks, probably because of the influence of an increasing water concentration in the continuous solution phase, similar to the situation in experiment 3. The PVM photo at 5 h 50 min reveals that at the end of the experiment the liquid phase was homogeneous, showing that the process had moved into region 3. The product crystal sieve size distribution is essentially bimodal, while the FBRM particle distribution is very irregular. The upper peak in the solid particle sieve size distribution (Figure 11) is attributed to agglomeration.

Product Size Distributions, Crystal Shapes, and Yield. In Figure 11, product size distributions and yields of each experiment are shown. Figure 11a shows the particle size distribution in each of the five experiments at the end of each experiment as recorded by the FBRM. The particles of experiment 1 show a well-formed log-normal or gamma-shaped distribution. For all other experiments, however, the product size distributions are more complex and irregular. The product particle size distribution from experiment 2 is better shaped compared to that of experiment 1, but the distribution is much wider and has a tendency to bimodality at about 200 and 400 μm. From experiment 3, the particles overall are fairly small—mainly below 400 μm with a tendency for the distribution to be bimodal. Nearly all the product particles of experiment 4 are also below 400 μm, but compared to the amount of crystals in experiment 3 the amount of crystals is much higher, and there is not a strong

dx.doi.org/10.1021/op200355b | *Org. Process Res. Dev.* 2012, 16, 1212−1224

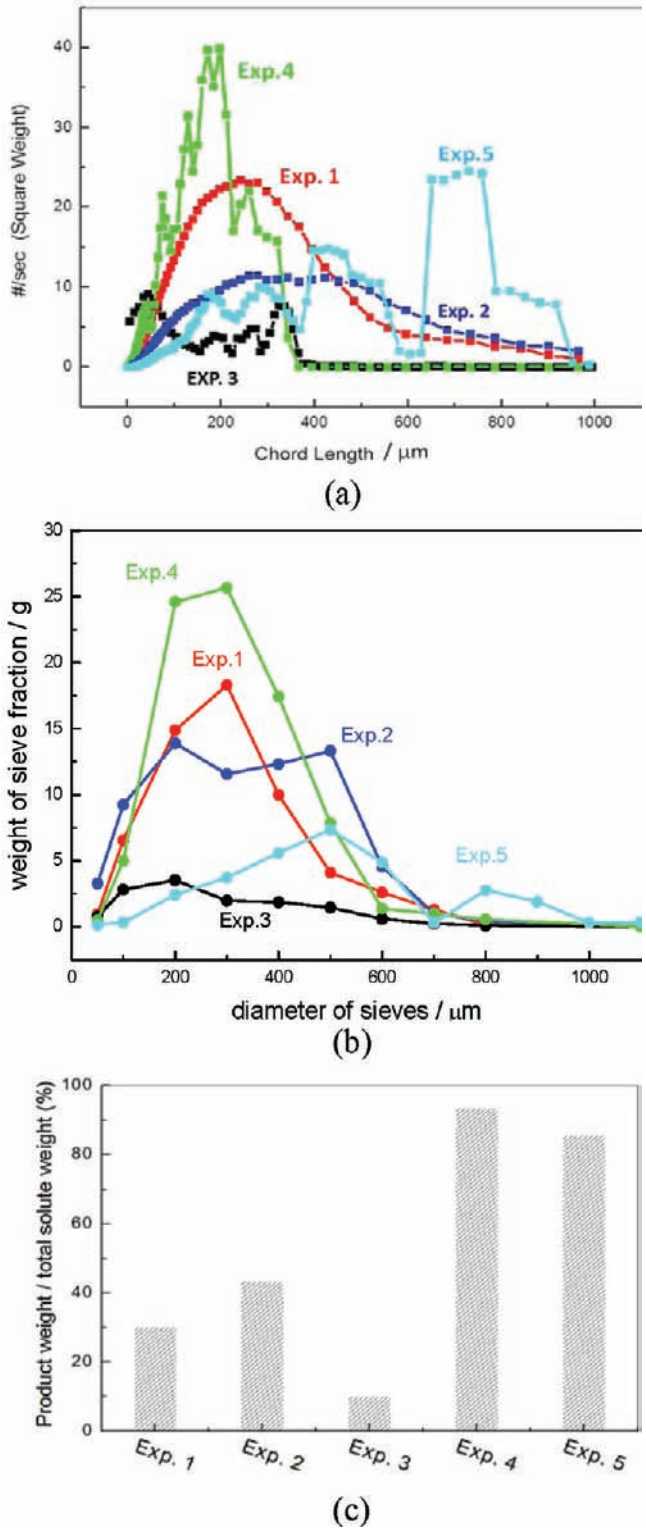

Figure 11. Product properties of the crystallization experiments: (a) FBRM curves, (b) weight of sieve fractions, (c) yield.

bimodality. The distribution of experiment 5 is very wide without any particular symmetry. In Figure 11b is presented the corresponding product particle size distribution as determined by sieving after filtration and drying. Differences between the Figure 11a,b distributions are because (i) the FBRM distributions are number distributions, while the sieve distributions are mass distributions; and (ii) the FBRM instrument measures the cord length distribution, while the sieving is normally assumed to separate the particles according to the second-largest dimension. However, in addition (iii) the FBRM curves actually also record liquid droplets in the suspension. Accordingly, if the process ends in a liquid−liquid phase-separated region, the recorded size distribution will include also the droplet size distribution. This explains the large difference in the overall shape of the size distributions for experiment 3, an experiment that terminates in the LLPS region 4. The particle size distribution of experiment 3 from FBRM shows a substantial number of particles below 100 μm, which are not found in the product particle size distribution determined by sieving. For the other four experiments the size distributions from the two methods are fairly similar. Figure 11c shows the yield of the crystallization experiments, calculated as the product dry solid weight/total mass of solute. Obviously the yield is higher in experiments 4 and 5, and the reason is the much lower solubility at the end point, which in turn is due to the lower concentration of ethanol. The yield of experiment 3 is very low as a result of the high solubility in the ethanol-rich liquid phase of the LLPS solution.

Product particles from the different experiments are shown in Figure 12. From experiment 1, which is the only experiment not experiencing liquid−liquid phase separation, we obtain the largest individual crystals and the least agglomeration. The material from experiment 5 contains very small crystals that are agglomerated into the larger particles recorded by FBRM and by the sieving analysis. The product of experiments 2 and 3 is somewhat in between experiments 1 and 5 with respect to agglomeration and crystal size. Comparing experiment 5 with experiment 4, the starting points in the ternary diagrams are not far from each other, but the agglomeration of crystals from experiment 5 is much stronger than among crystals from experiment 4, probably being the result of the low concentration of butyl paraben and higher concentration of water in experiment 5. Admittedly, additional crystallization experiments should be performed before the influence of liquid−liquid phase separation can be distinguished from the effect of the difference in solvent composition and supersaturation vs time profile, but from the limited results at hand it is observed that the largest individual crystals and the least agglomeration is obtained from that experiment where liquid−liquid phase separation is not occurring. In all four of the other experiments where liquid−liquid phase separation occurs, the crystals are smaller and more agglomerated, and the particle size distribution is wider or more irregular. However, another common feature among these four experiments, of course being a requirement for the phase separation to occur, is that the solution contains water—the presence of which can contribute to aggregation of hydrophobic faces of the butyl paraben crystals, and hence to the formation of agglomerates.

■ CONCLUSIONS

In pure water the butyl paraben solid−liquid solubility is below 1 mg/g, whereas in pure ethanol the solubility is more than 3 orders of magnitude higher. At low temperatures, the solubility of butyl paraben in homogeneous water−ethanol solutions increases with increasing ethanol concentration. However, in the temperature range of 20−30 °C, this dependency changes, leading to the highest solubility in homogeneous mixtures at 30−50 °C in a 70% by mass ethanol solution (on solute-free basis). Butyl paraben induces a liquid−liquid phase separation in the water−ethanol solution. This phase separation is clearly

dx.doi.org/10.1021/op200355b | Org. Process Res. Dev. 2012, 16, 1212−1224

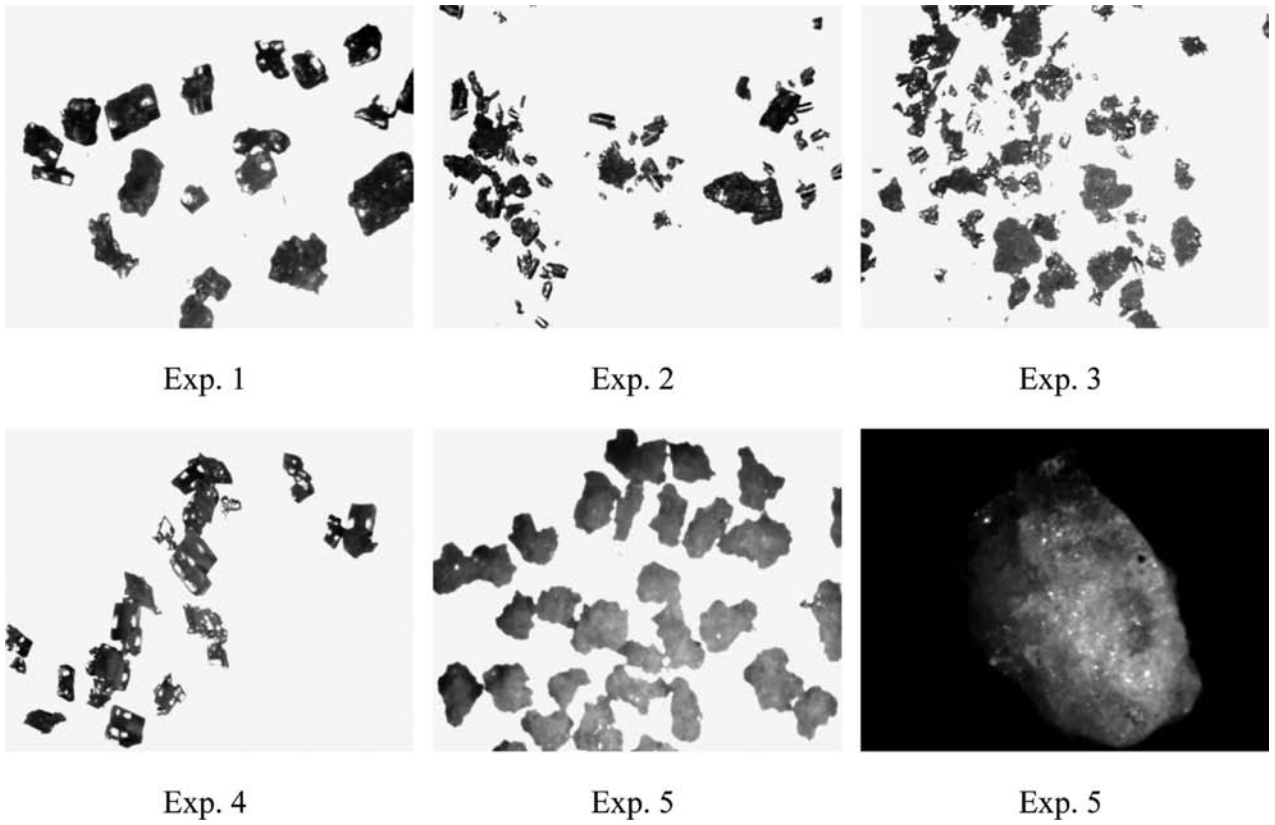

Figure 12. Product particles of the five cooling crystallization experiments. From upper left to lower right: microscopy photos with 20× magnification from experiments 1−5 and a single-particle photo with 90× magnification from experiment 5.

temperature dependent and solvent-composition dependent with an upper ethanol concentration slightly less than 70 wt % in the solvent mixture on solute-free basis, and a lower temperature limit between 10 and 1 °C.

Cooling crystallization experiments reveal that the product crystal size distribution depends significantly on the composition at the starting point. A liquid−liquid phase separation creates a solution having a higher butyl paraben concentration and a solution having a lower butyl paraben concentration. This leads to altered conditions for nucleation and crystal growth. In the results of the present study a process not traversing the liquid−liquid separation region generates the largest crystals with the least agglomeration and the best shaped size distribution. In all experiments where the solution is a mixture of water and ethanol and the process trajectory involves liquid−liquid phase separation, the individual crystals are smaller and more agglomerated, and the size distribution is less well shaped. However, whether this is due to the influence of the liquid−liquid phase separation or the presence of water in the solution or differences in the supersaturation vs time profile, remains to be clarified.

AUTHOR INFORMATION

Corresponding Author

*Telephone: +46 8790 8227. E-mail: akera@kth.se.

Notes

The authors declare no competing financial interest.

ACKNOWLEDGMENTS

Thanks to the support of Dr. Denise Crooker, University of Limerick, and the use of Mettler-Toledo equipment, the Solid State Pharmaceuticals Cluster, University of Limerick. H.Y. gratefully acknowledges the CSC scholarship from the Chinese government, and a scholarship from the Industrial Association of Crystallization Research and Development. Å.C.R. gratefully acknowledges the financial support of the Science Foundation Ireland.

REFERENCES

(1) Katta, J.; Rasmuson, C. Spherical Crystallization of Benzoic Acid. *Int. J. Pharm.* **2008**, *348* (1−2), 61−69.

(2) Di Martino, P.; Di Cristofaro, R.; Barthlemy, C.; Joiris, E.; Palmieri Filippo, G.; Sante, M. Improved Compression Properties of Propylphenazone Spherical Crystals. *Int. J. Pharm.* **2000**, *197* (1−2), 95−106.

(3) Niu, Y.; Yang, L.; Wang, H.; Wang, Z. Criteria of Process Optimization in Binary Polymer Blends with Both Phase Separation and Crystallization. *Macromolecules* **2009**, 1102−1105.

(4) Akaba, M.; Nojima, S. Effects of Phase Separation on the Crystallization Behavior in a Binary Blend of Poly(ε-caprolactone) Homopolymer and Poly(ε-caprolactone)-*block*-Polybutadiene Copolymer. *Polym. J.* **2005**, *37* (8), 584−591.

(5) Veesler, S.; Lafferrère, L.; Garcia, E.; Hoff, C. Phase Transitions in Supersaturated Drug Solution. *Org. Process Res. Dev.* **2003**, *7* (6), 983−989.

(6) Liu, Y.; Wang, X.; Ching, C. Toward Further Understanding of Lysozyme Crystallization: Phase Diagram, Protein-Protein Interaction, Nucleation Kinetics, and Growth Kinetics. *Cryst. Growth Des.* **2010**, *10* (2), 548−558.

(7) Veesler, S.; Revalor, E.; Bottini, O.; Hoff, C. Crystallization in the Presence of a Liquid-Liquid Phase Separation. *Org. Process Res. Dev* **2006**, *10* (4), 841−845.

(8) Deneau, E.; Steele, G. An In-line Study of Oiling Out and Crystallization. *Org. Process Res. Dev.* **2005**, *9* (6), 943−950.

(9) Gilles, F. New Perspectives for the On-line Monitoring of Pharmaceutical Crystallization Processes Using in Situ Infrared Spectroscopy. *Int. J. Pharm.* **2002**, *241* (2), 263−278.
(10) Dang, L.; Yang, H.; Black, S.; Wei, H. The Effect of Temperature and Solvent Composition on Transformation of β- to α-Glycine As Monitored in Situ by FBRM and PVM. *Org. Process Res. Dev.* **2009**, *13* (6), 1301−1306.
(11) He, G.; Tjahjono, M.; Chow, P. S.; Tan, R. B. H.; Garland, M. In Situ Determination of Metastable Zone Width Using Dielectric Constant Measurement. *Org. Process Res. Dev.* **2010**, *14* (6), 1469−1472.
(12) Hermanto, M. W.; He, G.; Tjahjono, M.; Chow, P. S.; Tan, R. B. H.; Garland, M. Calibration of Dielectric Constant Measurements to Improve the Detection of Cloud and Clear Points in Solution Crystallization. *Chem. Eng. Res. Des.* **2011**, *89* (12), 2613−2619.
(13) Simon, L. L.; Oucherif, K. A.; Nagy, Z. K.; Hungerbuhler, K. Histogram Matching, Hypothesis Testing, and Statistical Control-Chart-Assisted Nucleation Detection Using Bulk Video Imaging for Optimal Switching between Nucleation and Seed Conditioning Steps. *Ind. Eng. Chem. Res.* **2010**, *49* (20), 9932−9944.
(14) Barrett, M.; Hao, H.; Maher, A.; Hodnett, K.; Glennon, B.; Croker, D. In Situ Monitoring of Supersaturation and Polymorphic Form of Piracetam during Batch Cooling Crystallization. *Org. Process Res. Dev.* **2011**, *15* (3), 681−687.
(15) Simon, L. L.; Abbou Oucherif, K.; Nagy, Z. K.; Hungerbuhler, K. Bulk Video Imaging Based Multivariate Image Analysis, Process Control Chart and Acoustic Signal Assisted Nucleation Detection. *Chem. Eng. Sci.* **2010**, *65* (17), 4983−4995.
(16) DeVol, T.; Gohres, A.; Williams, C. Application of Classical versus Bayesian Statistical Control Charts to On-line Radiological Monitoring. *Journal of Radioanalytical and Nuclear Chemistry* **2009**, *282* (3), 933−938.
(17) Yang, H.; Rasmuson, C., Solubility of Butyl Paraben in Methanol, Ethanol, Propanol, Ethyl Acetate, Acetone, and Acetonitrile. *J. Chem. Eng. Data*, 25-38.
(18) Alexander, K. S.; Mauger, J. W.; Jr, H. P.; Paruta, A. N. Solubility Profiles and Thermodynamics of Parabens in Aliphatic Alcohols. *J. Pharm. Sci.* **1977**, *66* (1), 42−48.
(19) Perlovich, G.; Rodionov, S.; Bauer-Brandl, A. Thermodynamics of Solubility, Sublimation and Solvation Processes of Parabens. *Eur. J. Pharm. Sci.* **2005**, *24* (1), 25−33.
(20) Groen, H.; Roberts, K. Nucleation, Growth, and Pseudo-polymorphic Behavior of Citric Acid As Monitored in Situ by Attenuated Total Reflection Fourier Transform Infrared Spectroscopy. *J. Phys. Chem. B* **2001**, *105* (43), 10723−10730.
(21) Bonnett, P.; Carpenter, K.; Dawson, S.; Davey, R. Solution Crystallisation via a Submerged Liquid-Liquid Phase Boundary: Oiling Out. *Chem. Commun.* **2003**, *2003* (6), 698−699.
(22) Andersen, F. Final Report on the Safety Assessment of Methylparaben, Ethylparaben, Propylparaben, and Butylparaben. *Int. J. Toxicol.* **1984**, *3* (5), 147−209.
(23) Andersen, F. Final Report on the Safety Assessment of Isobutylparaben and Isopropylparaben 1. *Int. J. Toxicol.* **1995**, *14* (5), 364−372.
(24) Soni, M.; Burdock, G.; Taylor, S.; Greenberg, N. Safety Assessment of Propyl Paraben: A Review of the Published Literature. *Food Chem. Toxicol.* **2001**, *39* (6), 513−532.
(25) Soni, M.; Taylor, S.; Greenberg, N.; Burdock, G. Evaluation of the Health Aspects of Methyl Paraben: A Review of the Published Literature. *Food Chem. Toxicol.* **2002**, *40* (10), 1335−1373.
(26) Andersen, F. Final Amended Report on the Safety Assessment of Methylparaben, Ethylparaben, Propylparaben, Isopropylparaben, Butylparaben, Isobutylparaben, and Benzylparaben as used in Cosmetic Products. *Int. J. Toxicol.* **2008**, *27*, 1−82.
(27) Murrell, W.; Vincent, J. The Esters of 4-Hydroxybenzoic Acid and Related Compounds. IV. The Bacteriostatic Action of *n*-Alkyl 4-Hydroxybenzoates. *J. Soc. Chem. Ind.* **1950**, *69* (4), 109−113.
(28) Doron, S.; Friedman, M.; Falach, M.; Sadovnic, E.; Zvia, H. Antibacterial Effect of Parabens against Planktonic and Biofilm Streptococcus Sobrinus. *Int. J. Antimicrob. Agents* **2001**, *18* (6), 575−578.
(29) Golden, R.; Gandy, J.; Vollmer, G. A Review of the Endocrine Activity of Parabens and Implications for Potential Risks to Human Health. *Crit. Rev. Toxicol.* **2005**, *35* (5), 435−458.
(30) Ma, Y.; Marquis, R. Irreversible Paraben Inhibition of Glycolysis by Streptococcus Mutans GS-5. *Lett. Appl. Microbiol.* **2008**, *23* (5), 329−333.
(31) Charnock, C.; Finsrud, T. Combining Esters of Para-Hydroxy Benzoic Acid (Parabens) to Achieve Increased Antimicrobial Activity. *J. Clin. Pharm. Ther.* **2007**, *32* (6), 567−572.
(32) Perlovich, G. L.; Rodionov, S. V.; Bauer-Brandl, A. Thermodynamics of Solubility, Sublimation and Solvation Processes of Parabens. *Eur. J. Pharm. Sci.* **2005**, *24* (1), 25−33.
(33) Giordano, F.; Bettini, R.; Donini, C.; Gazzaniga, A.; Caira, M.; Zhang, G.; Grant, D. Physical Properties of Parabens and Their Mixtures: Solubility in Water, Thermal Behavior, and Crystal Structures. *J. Pharm. Sci.* **1999**, *88* (11), 1210−1216.
(34) Feng, Y.; Grant, D. J. W. Influence of Crystal Structure on the Compaction Properties of *n*-Alkyl 4-Hydroxybenzoate Esters (Parabens). *Pharm. Res.* **2006**, *23* (7), 1608−1616.
(35) Feng, Y.; Grant, D. J. W.; Sun, C. C. Influence of Crystal Structure on the Tableting Properties of *n*-Alkyl 4-Hydroxybenzoate Esters (Parabens). *J. Pharm. Sci.* **2007**, *96* (12), 3324−3333.
(36) Gauglitz, G.; Vo-Dinh, T., *Handbook of Spectroscopy*; Wiley-VCH: Weinheim, 2003.
(37) Grant, D.; Mehdizadeh, M.; Chow, A.; Fairbrother, J. Non-linear van't Hoff Solubility-Temperature Plots and Their Pharmaceutical Interpretation. *Int. J. Pharm.* **1984**, *18* (1−2), 25−38.
(38) Allexander, K.; Laprade, B.; Mauger, J.; Paruta, A. N. Thermodynamics of Aqueous Solutions of Parabens. *J. Pharm. Sci.* **1978**, *67* (5), 624−627.
(39) Yang, H.; Rasmuson, Å. C. Solubility of Butyl Paraben in Methanol, Ethanol, Propanol, Ethyl Acetate, Acetone, and Acetonitrile. *J. Chem. Eng. Data* **2010**, *55* (11), 5091−5093.
(40) Lafferrere, L.; Hoff, C.; Veesler, S. Study of Liquid-Liquid Demixing from Drug Solution. *J. Cryst. Growth* **2004**, *269* (2−4), 550−557.
(41) Thurston, G. Liquid-Liquid Phase Separation and Static Light Scattering of Concentrated Ternary Mixtures of Bovine α and β Crystallines. *J. Chem. Phys.* **2006**, *124*, 134909.